2nd Advanced Optical Metrology Compendium

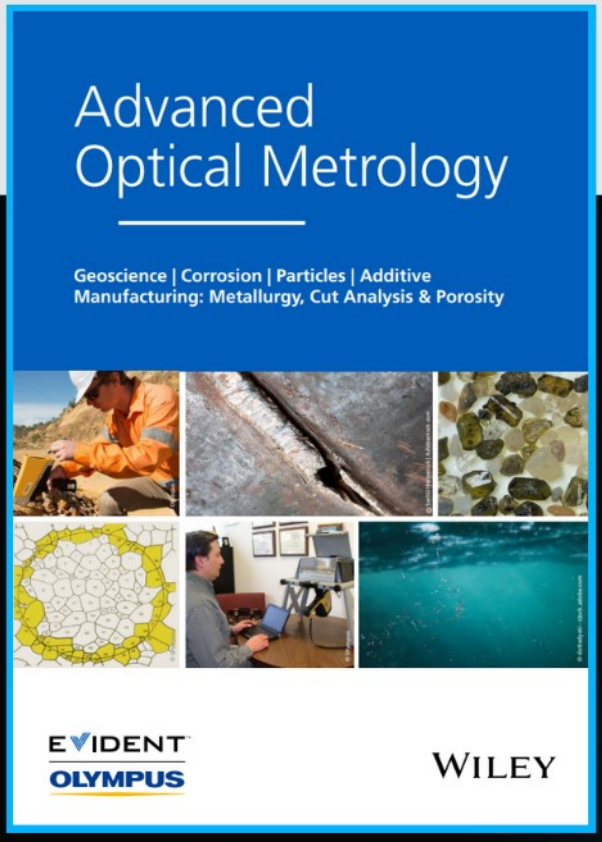

The latest eBook from Advanced Optical Metrology. Download for free.

This compendium includes a collection of optical metrology papers, a repository of teaching materials, and instructions on how to publish scientific achievements.

With the aim of improving communication between fundamental research and industrial applications in the field of optical metrology we have collected and organized existing information and made it more accessible and useful for researchers and practitioners.

EVIDENT
OLYMPUS

WILEY

ADVANCED FUNCTIONAL MATERIALS
www.afm-journal.de

Covalent Adaptable Microstructures via Combining Two-Photon Laser Printing and Alkoxyamine Chemistry: Toward Living 3D Microstructures

Yixuan Jia, Christoph A. Spiegel, Alexander Welle, Stefan Heißler, Elaheh Sedghamiz, Modan Liu, Wolfgang Wenzel, Maximilian Hackner, Joachim P. Spatz, Manuel Tsotsalas, and Eva Blasco**

Manufacturing programmable materials, whose mechanical properties can be adapted on demand, is highly desired for their application in areas ranging from robotics, to biomedicine, or microfluidics. Herein, the inclusion of dynamic and living bonds, such as alkoxyamines, in a printable formulation suitable for two-photon 3D laser printing is exploited. On one hand, taking advantage of the dynamic covalent character of alkoxyamines, the nitroxide exchange reaction is investigated. As a consequence, a reduction of the Young´s Modulus by 50%, is measured by nanoindentation. On the other hand, due to its "living" characteristic, the chain extension becomes possible via nitroxide mediated polymerization. In particular, living nitroxide mediated polymerization of styrene results not only in a dramatic increase of the volume (≈8 times) of the 3D printed microstructure but also an increase of the Young's Modulus by two orders of magnitude (from 14 MPa to 2.7 GPa), while maintaining the shape including fine structural details. Thus, the approach introduces a new dimension by enabling to create microstructures with dynamically tunable size and mechanical properties.

1. Introduction

Nowadays smart materials play a key role in a variety of pioneering advanced technological areas such as robotics[1–3] or in biomedicine.[4–6] Consequently, the demands for easily accessible smart materials, allowing processability in arbitrary structural shapes for individual applications is rising. Additive manufacturing emerged as the ideal technology for simple fabrication of customized 3D geometries, exhibiting different levels of complexity in the technologically relevant size regime between hundreds of nanometers to meters.[7] Focusing on the small regime, two-photon laser printing (2PLP), a photopolymerization based 3D printing technique, also known as 3D laser printing or direct laser writing (DLW), enables precise fabrication of complex 3D geometries in the micro- and nanometer regime.[8–12] The 2PLP technique employs a femtosecond pulsed near infrared laser, that is focused into a droplet of ink or photoresist, allowing 3D microstructure fabrication based on two-photon polymerization. This technique opens doors to feature sizes exhibiting sub-micrometer resolution and has already been successfully applied in different areas such as microrobotics,[13–15] microfluidics,[16,17] or microoptics.[18,19]

Y. Jia, A. Welle, S. Heißler, M. Tsotsalas
Institute of Functional Interfaces (IFG) Karlsruhe Institute of Technology (KIT)
76344 Eggenstein-Leopoldshafen, Germany
E-mail: manuel.tsotsalas@kit.edu

C. A. Spiegel, E. Blasco
Institute of Organic Chemistry
Heidelberg University
69120 Heidelberg, Germany
E-mail: eva.blasco@oci.uni-heidelberg.de

The ORCID identification number(s) for the author(s) of this article can be found under https://doi.org/10.1002/adfm.202207826.

DOI: 10.1002/adfm.202207826

C. A. Spiegel, E. Blasco
Centre for Advanced Materials
Heidelberg University
69120 Heidelberg, Germany

E. Sedghamiz, M. Liu, W. Wenzel
Institute of Nanotechnology (INT) Karlsruhe Institute of Technology (KIT)
76344 Eggenstein-Leopoldshafen, Germany

E. Sedghamiz
Schrodinger GmbH
68159 Mannheim, Germany

M. Hackner, J. P. Spatz
Department of Cellular Biophysics Max Planck Institute for Medical Research
69120 Heidelberg, Germany

M. Hackner, J. P. Spatz
Institute of Molecular Systems Engineering (IMSE) Heidelberg University
69120 Heidelberg, Germany

However, most inks were applied for 2PLP yield static structures, lacking any dynamic or "living" features. A strategy overcoming this limitation is the inclusion of stimuli response, also called 4D (micro)printing.[20–24] Stimuli-responsive materials such as hydrogels,[25–28] liquid crystal elastomers,[29,30] or shape memory polymers[31–33] have been extensively exploited. Another very promising approach – although still much less explored in the field of microprinting – is the incorporation of dynamic covalent chemistry[34–36] into the printed 3D microstructures.[37–39] Dynamic covalent chemistry allows reversible bond breakage and formation in the presence of a stimulus or in autonomous fashion. Polymer networks containing dynamic covalent bonds are able to assemble and disassemble reversibly under specific external stimuli, while being mechanically robust under ambient conditions. So far, a range of different dynamic covalent bond chemistries has been identified and utilized to create covalent adaptable networks[34,40–42] for a variety of applications such as polymeric reprocessability, self-healing materials, or solid-state plasticity based dynamic materials.[43–45]

The alkoxyamine bond is a particular example of dynamic covalent chemistry, as this bond offers the opportunity for nitroxide exchange reaction (NER) as well as nitroxide mediated polymerization (NMP),[46,47] incorporating dynamic, adaptive, and "living" properties to the polymeric networks.[41,48–55] However, despite of its versatility, this type of dynamic covalent chemistry has not been explored yet neither in additive manufacturing in general, nor in 2PLP in particular. Creating 3D microstructures consisting of covalent adaptable networks will open the path for direct modification of their molecular structure, allowing modulation of cross-linking density and mesh size postprinting. Thus, offering a switch to render key characteristics of printed microscopic objects, such as swelling degree or mechanical properties, e.g., Young's Modulus.

In this work, we report a novel pathway to produce such covalent adaptable microstructures (CAMs) offering precise adjustment of their mechanical properties by postprinting modification after structure fabrication. To achieve this, we combine 2PLP providing the highest degree of 3D fabrication precision with a simple ink system offering covalent dynamic bonds by incorporation of alkoxyamine functions into printed 3D microstructures (**Figure 1**a). Making use of the dynamic and living characteristics of this bond type, we modify the 3D

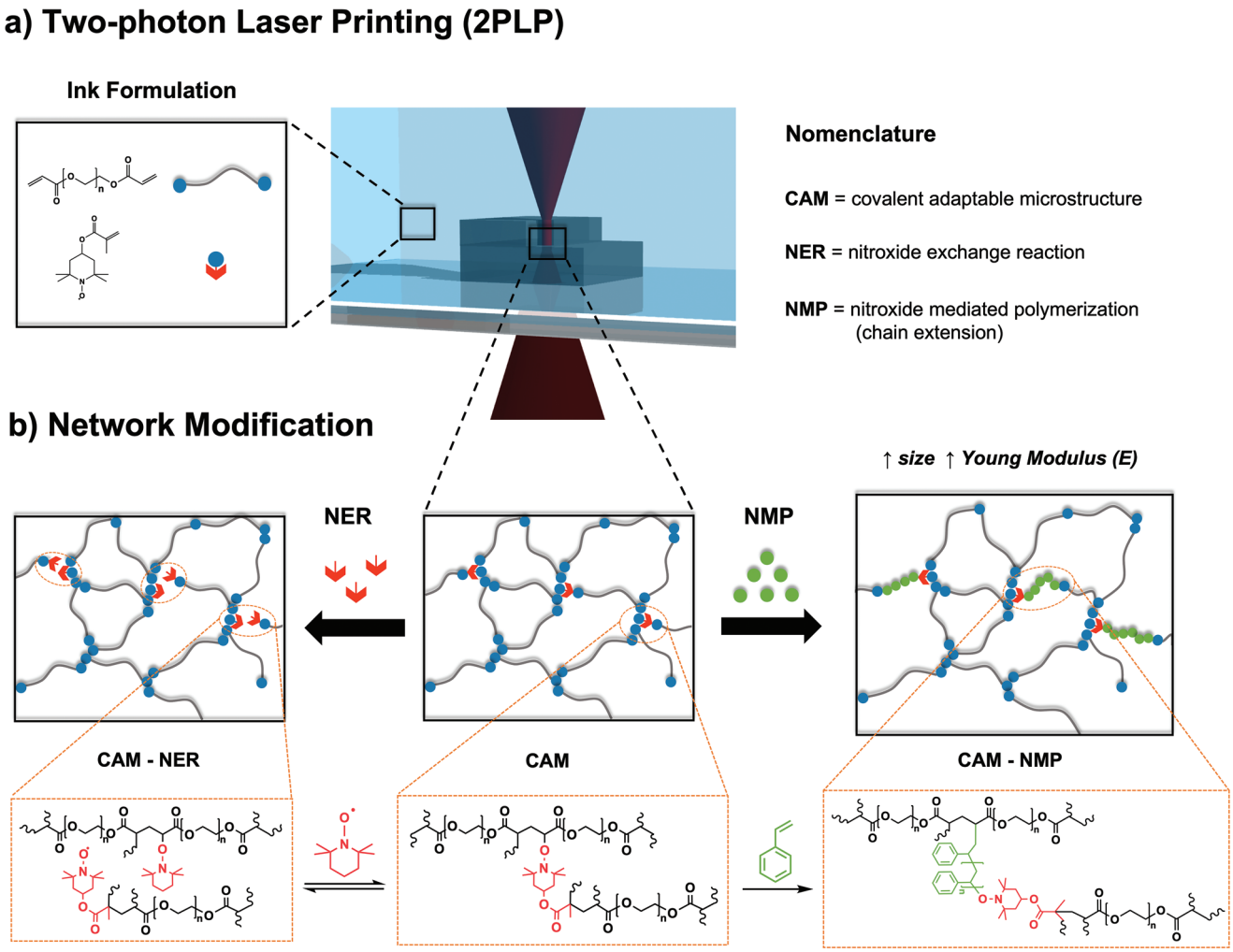

Figure 1. a) Schematic representation of the 3D laser printing process of alkoxyamine containing covalent adaptable microstructures (CAMs); b) Postprinting modification of CAMs via nitroxide exchange reaction (left, CAM-NER) and via nitroxide mediated polymerization (right, CAM-NMP).

microprinted structures by NER using additional nitroxide molecules (TEMPO) and by NMP using styrene as additional monomer for the extension (Figure 1b). Combining 2PLP technique with alkoxyamine chemistry will give access to entirely adaptable 3D microstructures, offering adjustment of their mechanical properties for custom applications in addition to precise fabrication at the molecular- and microscale.

2. Results and Discussion

2.1. Optimizing Ink Formulation for Two-Photon Laser Printing (2PLP) of Covalent Adaptable Microstructures (CAMs)

In order to incorporate the adaptivity feature, the inclusion of dynamic covalent bonds – alkoxyamine units in this case – into the printed structure is mandatory. With this aim, we selected commercially available TEMPO-methacrylate due to its dual functionality offering a stable nitroxide radical and a photopolymerizable methacrylate group, allowing for the later inclusion of alkoxyamine bonds into the printed covalent adaptable microstructures (CAMs). To ensure a stable network formation during laser microprinting, a multi-functional monomer is also required. Herein, poly(ethylene glycol) diacrylate (PEGDA, average M_n = 700 g mol^{-1}) was employed. As a photoinitiator, we chose 7-diethylamino-3-thenoylcoumarin (DETC), due to its well-known multi-photon initiation efficiency.[56] For complete dissolution of the mixture, including TEMPO-methacrylate, cross-linker and photoinitator, a solvent was necessary. Different high boiling point solvents, including dimethyl sulfoxide (DMSO), dimethylformamide (DMF) as well as diethyl formamide (DEF) and dimethylacetamide (DMAc), were tested (Table S1, Supporting Information). The cross-linker and photoinitiator mixture could readily be dissolved in all of these solvents, except for DMSO. It should be noted that the amount of solvent should be kept as low as possible for better printing performance. Thus, DMAc was chosen as the best candidate due to the good solubility for all components in the formulation.

After identification of suitable ink components, fine-tuning of the ratio between photoinitiator (DETC) and TEMPO-methacrylate was crucial. On one hand, the inclusion of nitroxide into the network forming the dynamic adaptive alkoxyamine bond is necessary to achieve the desired "living" features. On the other hand, the concentration of nitroxide is critical for successful printing. Nitroxides are commonly used as a radical quencher in polymerization processes. Thus, a considerable amount of TEMPO-methacrylate in the formulation can hinder the printing process leading to the necessity of high laser powers and slow printing speeds or even the impossibility to print. To balance the effect, we carefully optimized the printing formulation by varying the concentration of TEMPO-methacrylate and DETC (photoinitiator) (see **Table 1**). The 3D printability was first assessed by laser printing of simple cubic structures (dimensions ranging from $10 \times 10 \times 3$ to $42 \times 42 \times 30$ µm^3) at different laser powers and scan speeds. The laser printing experiments were performed using a commercially available set-up (Photonic Professional GT2, Nanoscribe GmbH). The details of the printed structures and conditions are also summarized in Table 1.

Initial tests starting with a 1:3 molar ratio between photoinitiator DETC and TEMPO-methacrylate (Ink C1) resulted in non-printability, due to radical inhibition of the free TEMPO radical and the high content of solvent necessary for complete dissolution of TEMPO-methacrylate and DETC. Decrease of TEMPO-methacrylate content toward a 1:1 ratio allowed printability at inefficient conditions (low scanning speeds) (Ink C2). By further increasing the photoinitiator content respective to TEMPO-methacrylate (2:1 molar ratio Ink C3, C4), the printability was improved. However, the formation of microbubbles during the laser printing process – most probably as a result of the local heat generated with the laser – hindered the reproducibility of the printing process. Subsequently, the photoinitiator concentration was decreased. It was found that the formulation with dramatically reduced photoinitiator content of below 1 wt.% and a 1:2 molar ratio between photoinitiator and nitroxide radical source (Ink C5) was printable with a scanning speed of 2500 µm s^{-1}, without microbubble formation, ideal for printing of more advanced structures exposing complex features. Attempts to increase the nitroxide radical source content while keeping similar levels of photoinitiator resulted in non-printability (Ink C6, C7) due to too strong quenching by the TEMPO moieties.

In addition, the 2PLP process including TEMPO-methacrylate was also studied through Coarse-Grained Molecular dynamics (CGMD) simulation using the Kremer-Grest model of polymers, along with the dynamic recombination of covalent

Table 1. Ink compositions and laser printing conditions.

Ink	DETC[a] [wt%]	PEG-DA 700 [wt%]	TEMPO-methacrylate [wt%]	DMAc [wt%]	Laser Power [mW]	Scan Speed [µm s^{-1}]	Crosslinker:PI:NO (molar ratio)[b]	Block Size (length, width, height) [µm]	Printability[c]
C1	2.1	70.1	4.6	23.2	–	–	15:1:3	–	–
C2	2.2	72.4	1.6	23.8	24	20	15:1:1	10, 10, 3	○
C3	5.5	59.2	2.0	33.3	22	400	10:2:1	32, 32, 6	◑
C4	3.7	61.0	1.2	34.1	23	600	15:2:1	42, 42, 10	◑
C5	0.9	92.4	1.5	5.2	48	2500	47:1:2	42, 42, 30	●
C6	0.9	91.4	2.7	5.0	–	–	47:1:4	–	–
C7	0.9	88.5	3.9	6.7	–	–	47:1:6	–	–

[a]photoinitiator; [b]molar ratio of PEG-DA (cross-linker), photoinitiator DETC (PI) and TEMPO-methacrylate (NO); [c]● printable, high scan speed; ◑ Printable, instabilities during writing, good scan speed; ○ printable with high risk of instabilities, low scan speed; – not printable.

bonds[57–60] In particular, two formulations (Ink C5 and Ink C6) were simulated. Both inks contain the same cross-linker/photoinitiator molar ratio (47:1), but a different TEMPO-methacrylate concentration. Experimentally, it was found that these differences are critical to achieve printability. Simulation results showed that during laser printing with Ink C5, the degree of conversion of the double bonds is as high as 80% (Figure S1, Supporting Information). In a stark contrast, the degree of double bond conversion was much lower (30%) for the composition ink C6 having a higher concentration of TEMPO-methacrylate. The simulations results are a good indication that small changes in the TEMPO-methacrylate concentration (just ≈1 wt.%) have large impact in the conversion degree and therefore, in the printing performance. Thus, due to its best printing performance Ink C5 including a crosslinker/photoinitiator/TEMPO-methacrylate 47:1:2 molar ratio was selected as suitable functional ink for subsequent studies.

2.2. Characterization of the Covalent Adaptable Microstructures (CAMs)

As a next step, we characterized the fabricated microstructures by FTIR microscopy and time-of-flight secondary ion mass spectrometry (ToF-SIMS), offering spatially resolved information on their chemical composition. For FTIR analysis we printed solid cuboid 3D microstructures (42 × 42 × 30 μm^3) using the optimized composition (Ink C5) – referred as CAMs – as well as 3D microstructures using a reference ink lacking of TEMPO-methacrylate – referred as Ref. In addition, we recorded the FTIR spectrum of the initial ink for comparison (**Figure 2**a). As expected, the characteristic bands at 1635 cm^{-1} and 980 cm^{-1} corresponding to the CH_2=CH stretching vibration of the unreacted monomers decreased dramatically, due to its consumption during printing. Also, the distinct absorption bands at 1720 cm^{-1}, assigned to the C=O stretching vibration from the conjugated α,β-unsaturated ester, shifts to 1730 cm^{-1} for the aliphatic ester, confirming successful polymerization for both CAM as well as Ref. Moreover, in the spectrum of the printed CAM we detected the absorption band at 1470 cm^{-1} for the CH_3 asymmetrical bending, which belongs to TEMPO-methacrylate moieties. This signal is not detected in the reference microstructures without TEMPO further supporting the successful incorporation of alkoxyamine moieties into the printed CAMs.

Time-of-flight secondary ion mass spectrometry (ToF-SIMS) allowed the identification of characteristic ion species for PEG ($C_2H_5O^+$) as well as alkoxyamine ($C_3H_8NO^+$). The reference microstructure and the CAM showed similar secondary ion count intensities for the PEG specific signal assigned to $C_2H_5O^+$ as both structures are primarily composed of PEG (Figure 2c). Contrarily, the alkoxyamine related signal corresponding to

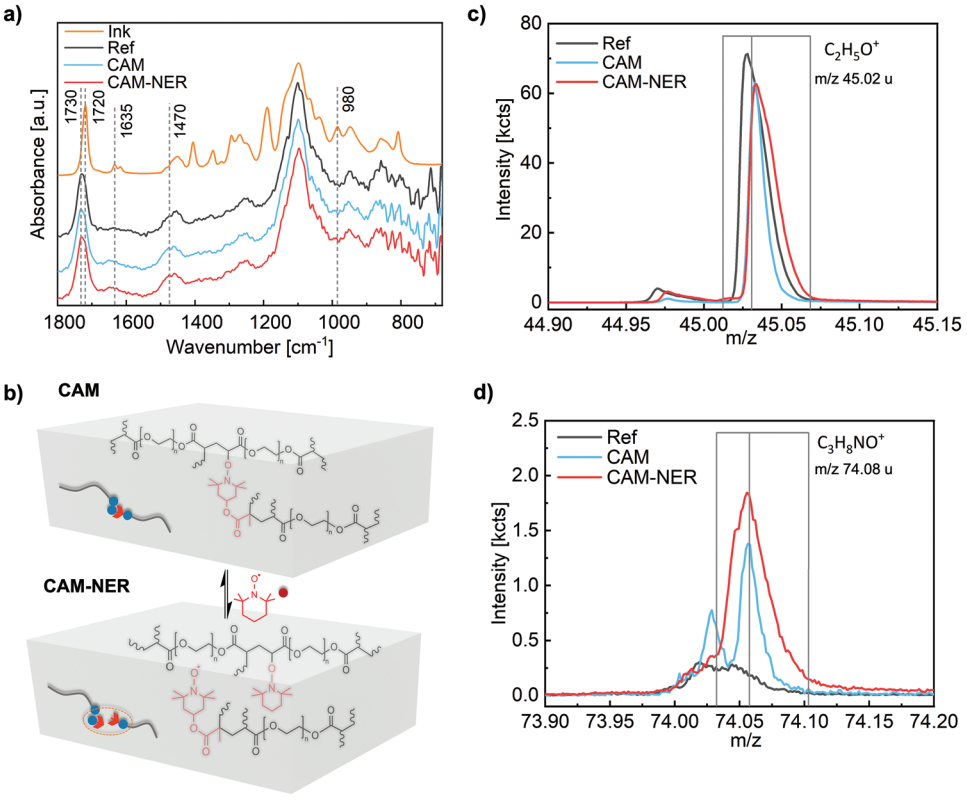

Figure 2. a) FTIR spectra of the ink (Ink), reference microstructure (Ref), CAM, and CAM-NER. The characteristic absorption bands corresponding to acrylate-moieties and alkoxyamine bonds are highlighted (gray dashed line); b) schematic illustration of nitroxide exchange reaction of CAM to CAM-NER; c) ToF-SIMS spectra of reference microstructure (Ref), CAM, and CAM-NER in the region of PEG specific ($C_2H_5O^+$) signals; d) ToF-SIMS spectra of Ref, CAM, and CAM-NER in the region of alkoxyamine specific ($C_3H_8NO^+$) signals.

the ion $C_3H_8NO^+$ was only observable for the CAM structure (Figure 2d), further supporting the presence of alkoxyamine groups within the network. Figure S4b (Supporting Information) and Figure S5b (Supporting Information) visualizes the differences in chemical composition of CAM and reference cuboid microstructures based on the $C_2H_5O^+$ and $C_3H_8NO^+$ signal intensities.

2.3. Postprinting modification of the Covalent Adaptable Microstructures (CAMs)

Having established and optimized the methodology for 2PLP of covalent adaptable microstructures (CAMs), we exploited the dynamic covalent character of the alkoxyamine bond by performing Nitroxide Exchange Reaction (NER) as well as the possibility to introduce new monomers via Nitroxide Mediated Polymerization (NMP) chain extension.

2.3.1. Nitroxide Exchange Reaction (NER)

It is expected that the NER leads to an overall lower cross-linking density in the product (CAM-NER) and a higher overall TEMPO content compared to the original CAM (Figure 2b). In order to test our hypothesis, the printed CAMs were heated in the presence of an excess of free TEMPO molecules and characterized by FTIR microscopy and ToF-SIMS. As the PEG chains are still present in large excess within the CAM-NER structure, we did not observe obvious changes in the IR-microscopy spectra comparing CAM and CAM-NER microstructures, confirming overall preservation of the CAM after NER postprinting modification. However, the ToF-SIMS spectrum of CAM-NER showed an increase in the secondary ion count intensities of $C_3H_8NO^+$ species compared to the original CAM (Figure 2d). The signal of the PEG characteristic ion species $C_2H_5O^+$ showed similar intensities for CAM and CAM-NER structures, since the PEG polymer chain is unaffected by the inclusion of additional nitroxide radicals and the reduction of cross-linking density (Figure 2c). Visible observation of CAM and CAM-NER blocks exhibited a slight indentation of the CAM-NER hinting toward softening of the structures due to less cross-linking within the network (Figure S4b, Supporting Information).

To investigate in depth the effect on the mechanical properties of CAM-NER we performed nanoindentation measurements, providing access to mechanical properties such as the reduced Young's Modulus and the hardness. The nanoindentation measurements were carried out on the previously printed cuboid 3D microstructures. We observed a lower reduced Young's Modulus of 7.2 ± 1.3 MPa for CAM-NER compared to 14.3 ± 0.6 MPa for the initial CAM (Figure S2, Supporting Information). We also observed a similar trend in the hardness showing 1.4 ± 0.2 MPa for CAM-NER and 2.7 ± 0.3 MPa for CAM. The lower hardness and reduced Young's Modulus can be assigned to the lower overall cross-linking density, resulting from the exchange reaction. It should be noted that the 3D shape of the printed microstructure is retained after NER postprinting modification.

2.3.2. Nitroxide Mediated Polymerization (NMP) Chain Extension

Taking advantage of the living characteristics of the alkoxyamine bond we investigated the possibility to incorporate new monomers into the printed CAM network via controlled NMP. We selected styrene as monomer for chain extension for two reasons: i) it is well established for NMP and ii) styrene derivatives have not been reported as printable monomer for 2PLP and this will enable the incorporation of new materials in the 3D printed microstructures. In addition, the mechanical properties of polystyrene differ strongly from PEG, which is the main component of the printed CAM. In contrast to rubber like PEG networks, styrene is at room temperature in glassy state. Thus, we anticipate a clear increase in reduced Young's Modulus and hardness for CAM-NMP compared to the initial PEG-based CAM.

For the NMP chain extension of the CAMs, we immersed the printed microstructures in degassed styrene, sealed the reaction vial under inert conditions, and performed NMP at 130 °C at different reaction times. After NMP polymerization, characterization by FTIR microscopy revealed the presence of characteristic bands for polystyrene. New bands in the spectrum of CAM-NMP for both alkyl C—H stretching vibrations at 2920 cm^{-1} and aromatic C=C stretching vibrations at 1601, 1492, 1450 cm^{-1} as well as C—H out-of-plane bending vibrations at 758 and 699 cm^{-1} are strong evidence for the successful incorporation of polystyrene chains in the CAM network by NMP chain extension (**Figure 3**a,b).

To further confirm the successful incorporation of polystyrene we performed ToF-SIMS. We observed a strong and distinct signal of the tropylium cation $C_7H_7^+$, characteristic for the presence of polystyrene, in the CAM-NMP network (Figure 3d). The appearance of the strong signal for the tropylium cation goes along with a dramatic drop of the PEG signal intensity ($C_2H_5O^+$) due to the dilution effect of the additionally incorporated polystyrene chains (Figure S4a, Supporting Information). Thus, in the ToF-SIMS image of CAM-NMP (Figure S4b, Supporting Information) the microstructures can be barely identified. The same dilution effect leads to the decrease of the secondary ion count intensities for the alkoxyamine specific $C_3H_8NO^+$ signal in the CAM-NMP compared to the CAM (Figure S5, Supporting Information). Furthermore, we observed a dramatic increase in volume for the CAM-NMP compared to the structure of CAM (Figure S6, Supporting Information), supporting the successful NMP chain extension.

Having established as a solid procedure for incorporation of polystyrene chains by NMP postprinting modification of the printed CAMs, we investigated the effect of polystyrene incorporation on the mechanical properties by nanoindentation. For this purpose, we performed the NMP chain extension with styrene for two reaction times, 2 and 4 h, and evaluated the reduced Young's Modulus as well as hardness for each sample. Compared to the initial values for the CAM microstructures (14.3 ± 0.6 MPa for the reduced Young's Modulus and 2.7 ± 0.3 MPa for the hardness), CAM-NMP microstructures exhibited an increase of two orders of magnitude for both properties, resulting in a reduced Young's Modulus of 2660.6 ± 108.1 MPa and a hardness of 201.3 ± 26.4 MPa after 2 h of reaction time. After 4 h, similar values were observed

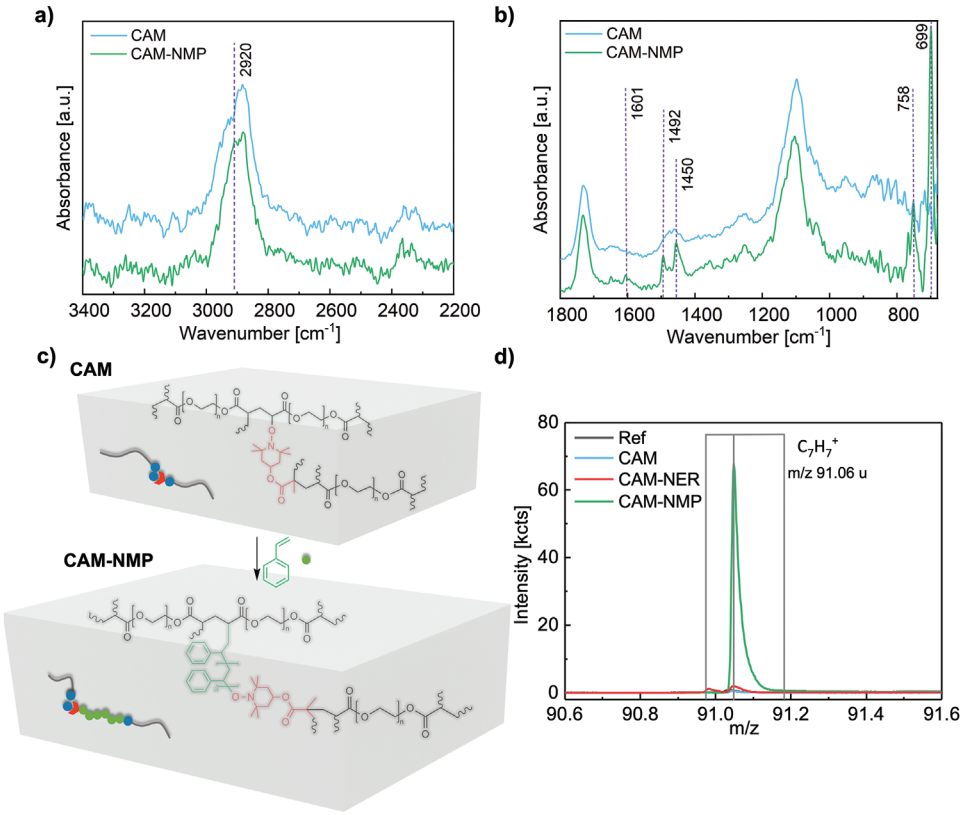

Figure 3. a) FTIR spectra of CAM and CAM-NMP. The characteristic absorption peaks of polystyrene are highlighted (purple dashed lines); b) FTIR spectra of CAM and CAM-NMP. The characteristic absorption peaks of polystyrene are highlighted (violet dashed lines); c) schematic illustration of nitroxide mediated polymerization of CAM to CAM-NMP; d) ToF-SIMS spectra of $C_7H_7^+$ ion species. This species does not appear in spectra of reference microstructure (Ref), CAM, and CAM-NER. Only CAM-NMP has a distinct strong $C_7H_7^+$ peak.

for both reduced Young's Modulus and hardness proving the successful incorporation of polystyrene, now dominating the mechanical properties. All nanoindentation data and SEM images of the measured samples are depicted in Figure S3 (Supporting Information).

The mechanical properties of CAM, CAM-NER, and CAM-NMP were also investigated using Molecular Dynamics (MD) simulation. Figure S7 (Supporting Information) shows the post polymerized microstructure CAM-NMP and the simulated stress–strain curves of three microstructures. The calculated Youngs' Moduli were 0.14, 0.064, and 4.5 $\varepsilon\,\sigma^{-3}$ respectively. The significant increase in mechanical properties for CAM-NMP is attributed to the longer, highly entangled polystyrene chains. Earlier theoretical studies have also shown that polydispersity in strand length is expected to control the mechanical strength of polymer networks.[61]

2.4. Toward "Living" 3D Complex Microstructures

To prove the versatility and the potential of the developed approach, we demonstrated the dynamic feature and extension reaction of alkoxyamine units in more complex 3D geometries. In particular, three different 3D models, a sunflower, an octopus, and a gecko were printed using the optimized formulation including TEMPO methacrylate (**Figure 4**). The microstructures were printed on glass substrates functionalized with a methacrylate silane to ensure good adhesion during the post-functionalization processes. The good printing quality of the process can be appreciated in the fine features such as the disk florets in the middle of the sunflowers or arms and eyes of the octopus. In case of the geckos structurally demanding features such as the legs were fabricated in a quality that allows to distinguish between the single toes. As a second step, NMP chain extension with styrene was carried out at different reaction times. As visible in Figure 4a, the micrometric sunflower, resulted in a PS-containing flower exhibiting great structural quality despite the impressive size growth in volume, visible in the increase in diameter of ≈15% after 2 h and 75% after 4 h NMP. Interestingly a homogeneous growth was achieved, allowing to differentiate between the smallest features of the original microscopic flower. We also conducted the same chain extension procedure on printed micrometric octopodes and geckos. In case of the octopodes we observe an enormous volume extension of the whole structure especially visible at the legs and the head after 2 and 4 h polymerization. From head dimension comparison between all three states we found an approximate size increase of 69% after 2 h and 114% after 4 h NMP. Despite this growth structural features such as the arms or the shape of the head and eyes were maintained. The geckos displayed excellent growth and structural maintenance as well. Comparing demanding features such as the legs with

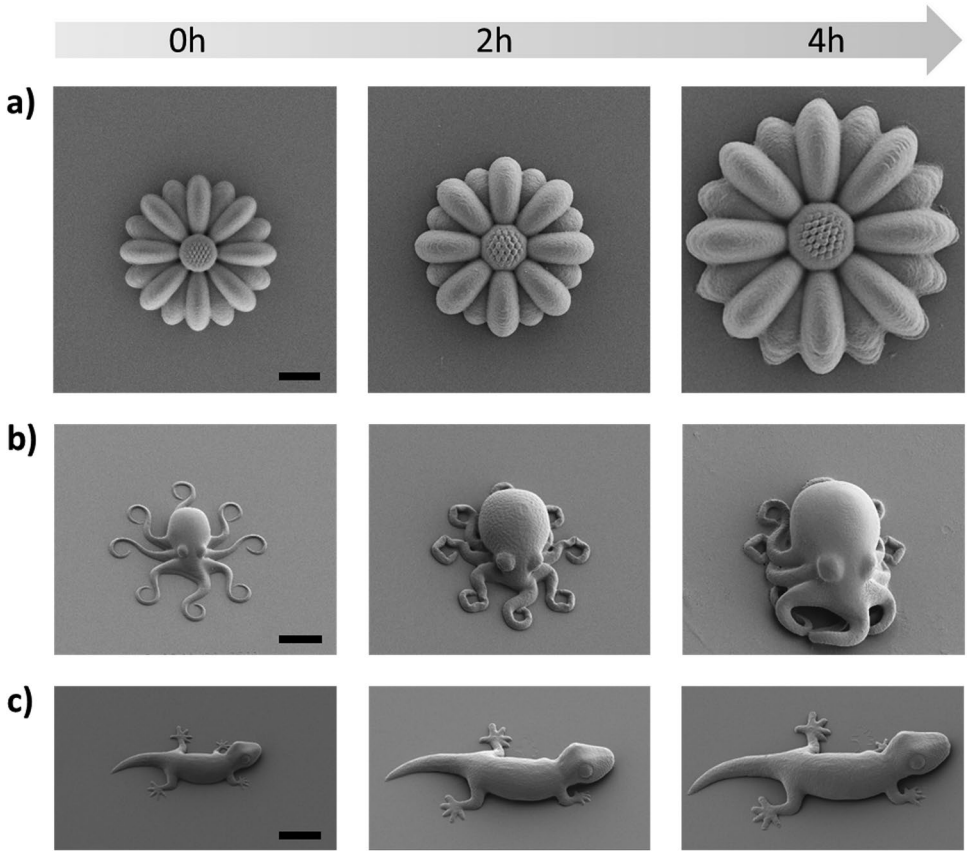

Figure 4. NMP chain extension of complex CAM microstructures with styrene at different reaction times. a) Top view SEM images of a CAM sunflower (left) and after 2 h (middle) and 4 h (right) reaction time; b) Tilted SEM images (30°) of a CAM octopus (left) and after 2 h (middle) and 4 h (right) reaction time; c) Tilted SEM images (30°) of a CAM gecko (left) and after 2 h (middle) and 4 h (right) reaction time. All images within one structure type were recorded for size comparison at similar magnification. Scale = 20 µm for all images.

their fingers or the eyes the 4 h gecko can be seen as an almost perfect copy of the smaller gecko, but larger and stiffer. The size growth was ≈52% after 2 h and 76% after 4 h postprinting modification time.

3. Summary and Conclusion

We have introduced a new approach for the preparation of covalent adaptable microstructures (CAMs) by 2PLP. The "living" feature of our system is based on the inclusion of dynamic alkoxyamine bonds into the polymeric network allowing for nitroxide exchange reaction (NER) and chain extension via nitroxide mediated polymerization (NMP). To achieve this, we carefully designed an ink system based on PEGDA-700 as cross-linker and TEMPO-methacrylate and DETC as photoinitiator. It was found that the concentration of photoinitiator as well as the ratio between TEMPO-methacrylate and photoinitiator were critical to achieve good printability. The successful incorporation of the alkoxyamine units into the laser printed microstructures as well as the NER and NMP chain extension were evidenced by FTIR spectroscopy and ToF-SIMS. By NER, a reduction of mechanical properties of ≈50% for the reduced Young's Modulus and hardness was achieved while maintaining structural quality. By NMP chain extension using styrene as a monomer, we observed a large increase in mechanical properties in the range of 2 orders of magnitude for the reduced Young's Modulus and hardness while preserving the initial 3D shape. Thus, the reported novel functional ink system combines high fabrication precision of 2PLP with dynamic and adaptable features on demand such as size and mechanical properties, which are unattainable with conventional formulations. We especially envision new opportunities in different fields of applications including microrobotics, microfluidics, or biomedicine, where precise fabrication along with specific adjustment of mechanical properties is of highest necessity.

4. Experimental Section

Materials and Characterization: All chemicals were used without further purification. Poly(ethylene glycol) diacrylate (average M_n = 700 g mol^{-1}, PEGDA-700), 4-methacryloyloxy-2,2,6,6-tetramethylpiperidine-1-oxyl (97%, TEMPO-methacrylate) were purchased from Sigma Aldrich. 7-diethylamino-3-thenoylcoumarin (98%, DETC) was obtained from Alfa Chemistry. Dimethylacetamide (99%, DMAc) was purchased from VWR. Styrene (99%) was obtained from Merck. Additional solvents used for development and postprinting modification were obtained from Sigma Aldrich and VWR. Sylgard 184 (Dow) was purchased from Farnell.

Ink Preparation: TEMPO-methacrylate (8.24 mg, 0.0342 mmol) and DETC (5.00 mg, 0.0152 mmol) were added to a brown glass vial and suspended in PEGDA-700 (500 mg, 0.714 mmol, 446 µL) and DMAc (28.2 mg, 0.323 mmol, 30 µL). After sonication until complete dissolution of TEMPO-methacrylate and DETC, examination of the final ink under microscope was conducted to ensure absence of insoluble particles at the microscopic regime. The ink was stable and printable over several months of storage at rt in darkness or yellow light conditions.

Sample Preparation: Using a commercial 2PLP sample holder (Nanoscribe) for oil immersion mode methacrylate-functionalized glass slides were attached by tape. Immersion oil was added on the unfunctionalized glass slide surface, a hole containing PDMS frame was placed on the methacrylate-functionalized side of the glass slide. The functional ink was added into the hole of the frame, that was closed by placement of glass on top of it, ensuring in this way as far as possible air exclusion. The sample was utilized directly for microprinting. The entire sample preparation was performed under yellow light conditions.

PDMS Mold Preparation: Base and cross-linker components of commercial Sylgard 184 silicone elastomer were mixed in a 10:1 weight ratio and stirred for 10 min to ensure homogeneous mixing. After removal of all air bubbles under reduced pressure, a clear viscous solution was obtained. The solution was filled into plastic petri dishes and cured for 24 h at rt.

Substrate Functionalization: To improve adhesion of 3D printed microstructures glass slides (Marienfeld, 170 ± 5 µm strength) were washed first with isopropanol, then with acetone, and dried using pressurized N_2. Subsequently, the surface was cleaned and activated for 1 min by plasma treatment. Following this, the glass slides were immersed in a 4×10^{-3} M solution of 3-(trimethoxysilyl)propyl methacrylate in toluene for 1.5 h. After washing twice in toluene and once in acetone and successive drying by pressurized N_2, the methacrylate-functionalized glass slides were used as substrates for 2PLP microfabrication. The entire substrate functionalization and subsequent storage were performed under yellow light conditions.

Postprinting Modifications: CAM-NER: The printed CAMs were placed in a sealed vessel with an excess of 2,2,6,6-tetramethylpiperidine-1-oxyl (TEMPO) (20.0 mg, 0.128 mmol), degassed toluene (1.80 mL, 1.56 g, 0.0170 mol), and methanol (0.200 mL, 0.158 g, 0.00493 mol) under N_2 atmosphere and heated to 100 °C inside an oven. After 8 h reaction time, the samples were washed using THF and isopropanol to remove unreacted TEMPO. Afterwards CAM-NER samples were dried under vacuum and stored under ambient conditions.

Postprinting Modifications: CAM-NMP: Nitroxide mediated polymerization (NMP) was performed by the addition of degassed styrene (2.00 mL, 1.82 g, 0.0175 mol) to a sealed reaction vessel containing the printed CAMs under N_2 atmosphere. After heating for 130 °C inside an oven for prior described reaction times, the samples were washed in THF and isopropanol to remove unreacted styrene, dried under vacuum, and stored under ambient conditions.

Two-Photon Laser Microprinting (2PLP): 2PLP was performed utilizing a commercial Photonic Professional GT 2 (Nanoscribe GmbH) direct laser writing system. Fabrication of all microstructures was performed in oil immersion mode using a 63× oil immersion objective (NA = 1.4). GWL files for desired geometries were either coded directly or generated from STL files of 3D structures employing commercial Describe software (Nanoscribe). Slicing was set for blocks to 350 nm and hatching to 300 nm. For complex 3D structures optimized values of 200 nm for slicing and 300 nm for hatching were used. The laser power and scanning speeds were optimized for each structure type individually. The fabricated microstructures were developed for 10 min in acetone and subsequently 1 min in isopropanol, followed by drying under ambient conditions. The printed samples were stored under ambient conditions. Microprinting and development was performed under yellow light conditions.

Attenuated Total Reflection Fourier Transform Infrared (ATR-FTIR): A Bruker Optics Tensor 27 spectrometer with room temperature deuterated triglycinesulfate (RT-DTGS) detector and a Bruker Optics Platinum ATR accessory (diamond crystal with one reflection) were used (Bruker Optics, Ettlingen, Germany). The ink, consisting of PEG-DA, DETC, TEMPO-methacrylate, and DMAc, was placed on the diamond crystal directly without any additional sample preparation. The spectrum was recorded at room temperature (≈22 °C) from 4000 to 400 cm^{-1} with a resolution of 4 cm^{-1} against an air background. The absorption band positions are given in wave numbers $\tilde{\nu}$ (cm^{-1}).

FTIR Microscopy: For FTIR Microscopy a Bruker Hyperion 3000 FTIR Microscope (Bruker Optics GmbH Ettlingen, Germany) equipped with a mid band MCT-detector cooled by liquid nitrogen was used. The measurements of the structured micro samples were done by using a Bruker 20x ATR-objective with a Ge-crystal tip resulting in a field of view of ≈40 μm^2. The contact pressure on the sample was set to 0.5 N. Sixty four scans were integrated for each spectrum, all spectra were measured against an air background with a bandwidth of 650–4000 cm^{-1}, all samples were examined in the dried state.

Time-of-Flight Secondary Ion Mass Spectrometry (ToF-SIMS): ToF-SIMS of reference microstructure (Ref), CAM, CAM-NER and CAM-NMP was performed on a TOF.SIMS5 instrument (ION-TOF GmbH, Münster, Germany), all samples were measured in the dried state. The instrument features a Bi cluster primary ion source and a reflectron type time-of-flight analyzer. UHV base pressure was $<5 \times 10^{-8}$ mbar. For high mass resolution investigation, the Bi source was operated in the "high current bunched" mode, providing short Bi^+ primary ion pulses at 25 keV energy, a lateral resolution of ≈4 µm, and a target current of 0.35 pA. The short pulse length of 1.0 ns enabled a high mass resolution. The primary ion beam was usually rastered across a 500×500 μm^2 field of view on the sample, and 256 pixels were recorded. Spectra were calibrated using the omnipresent C^-, C_2^-, C_3^-, or the C^+, CH^+, CH_2^+, and CH_3^+ peaks. Based on these datasets, the chemical assignments for characteristic fragments were determined. For high lateral resolution imaging, the primary ion source was operated in "delayed extraction" mode. In this mode, the lateral resolution of the instrument is in the range of 150 nm, and this mode provides a good mass resolution of >4000 m Δm^{-1}. Here, in "delayed extraction" mode, a concentric field of 100×100 μm^2 on reference microstructure, CAM, CAM-NER, or a concentric field of 200×200 μm^2 on CAM-NMP were analyzed respectively, and 256×256 data points for all samples were recorded.

Nanoindentation: Nanoindentation of reference microstructure CAM, CAM-NER, and CAM-NMP was performed by application of a trapezoid loading function with a loading and unloading rate of 200 nm s^{-1} up to 1 µm and a plateau time of 2 s. The measurement was performed on dried samples with a diamond Berkovich tip and automatic drift control. For each sample type (CAM, CAM-NER, and CAM-NMP) n = 10 measurements were carried out and a mean value with standard deviation was calculated from the obtained results. Values for the reduced Young's Modulus and the hardness were calculated according to published work.[62]

Sputter Coating: Block samples were sputter coated with a 10 nm layer of graphite. Complex 3D structures were sputter coated with 12 nm layer of Pd:Pt.

Scanning Electron Microscopy (SEM): SEM of all fabricated structures was performed with Zeiss Ultra 55 (Carl Zeiss AG) at 3 kV.

Simulation of Cross-linking Process: Formation of 3D polymer network from polymer chains has been simulated using a Coarse-Grained Molecular Dynamics (CGMD) simulation approach. The simplest model for an elastomer that can capture the essential features of a rubbery (elastomer) material at the atomic scale is the model developed by Kremer and Grest.[63] It was assumed that all the particles in the system have identical masses (m) and interact via a truncated Lennard–Jones 6–12 potential equilibrated as the polymer melts. The ε and σ parameters were set to unity and were the same for all monomers. The cutoff distance for the bead-bead interactions was set to $r_{cut} = 2.5\ \sigma$ at a number density $\rho = 0.85$.[64] Finite extensible nonlinear elastic (FENE) potential with the spring constant $k_{spring} = 30\ k_BT\ \sigma^{-2}$ and the maximum bond length $R_{max} = 1.5\ \sigma$[63] was employed to maintain the connectivity of the network. The repulsive part was represented by truncated-shifted Lennard–Jones (LJ) potential with $r_{cut} = 21/6\ \sigma$ and $\varepsilon_{LJ} = 1.5\ k_BT$. A monomer could react with an active monomer within a certain

probability if the distance of the selected bead was <1.15 σ (reaction radius) from an active monomer. The initial configuration of the CGMD was a simulation box of 30 × 30 × 30 σ, consisting of 1000 PEG-DA chains, in Figure S1 (Supporting Information). During the equilibration, the NVE ensemble was adopted and periodic boundary conditions were applied on three dimensions. Large-scale atomic/molecular massively parallel simulator (LAMMPS) software developed by Sandia National Laboratories had been employed for all simulations.[63] After fabricating the 3D polymer networks, they were relaxed for at least 5 × 104 τ_{LJ} in NPT ensemble. The temperature was maintained to be constant by coupling the system to a Langevin thermostat.[65]

To calculate Young's Modulus, a set of uniaxial tensile deformations were performed to obtain the stress–strain curves. The uniaxial deformation was realized by stepwise stretching the simulation box with $\Delta t = 0.01\ \tau$ along the *x*-axis and at the same time compressing the box along L_z and L_y appropriately to maintain the simulation box being constant. A constant engineering strain rate of $\nu = 0.001\ \tau^{-1}$ was employed during the tensile process that caused the box dimension to change linearly with time in one dimension.[66,67] More detailed information on stress–strain simulations and Young's Modulus calculations can be found in reference.[68]

Construction of CG Model: PEGDA chains were modeled by 14 PEG monomers with one acrylate monomer attached to each end. The mixture of PEGDA, photoinitiator, and TEMPO was built in a stoichiometric ratio 47:1:2 and 47:1:4. With the 47:1:4 ratio no stable polymer network had been obtained which is in line with the experimental observations (see Figure S1, Supporting Information). Therefore 47:1:2 ratio had been used for all simulations. The mapping scheme is shown in Figure S8 (Supporting Information). Since each photoinitiator splits into two active radicals after laser irradiation, each photoinitiator molecule were presented by two active monomers in the simulations. Three simulation boxes had been made, a first one consists of unreacted mixture of 1000 PEG-DA chains, photoinitiator, and TEMPO-methacrylate. Active photoinitiators start the cross-linking reactions, e.g., acrylate-acrylate and acrylate-TEMPO and simulation runs until no more bonds can be formed. A second one for the same mixture but the probability that a TEMPO participates in the reactions is much lower than the first simulation. Therefore, most of the TEMPO beads remain unreacted. A third one for the mixture of cross-linked PEGDA, TEMPO, photoinitiator, and styrene. The three simulation boxes represent CAM, CAM-NER, and CAM-NMP respectively.

Supporting Information

Supporting Information is available from the Wiley Online Library or from the author.

Acknowledgements

Y.J. and C.A.S. contributed equally to this work. E.B.acknowledges the funding from the Deutsche Forschungsgemeinschaft (DFG, German Research Foundation) via the project BL-1604/2-1. The authors also thankthe Excellence Cluster "3D Matter Made to Order" (EXC-2082/1-390761711) and the Carl Zeiss Foundation through the "Carl-Zeiss-Foundation-Focus@HEiKA" for funding. The authors further acknowledge the support by the Helmholtz program "Materials Systems Engineering" (MSE) at the Karlsruhe Institute of Technology and the Max Planck Society for general support. The authors thank Prof. Dr. R. Schöder for the access to SEM. The authors also want to thank Prof. Dr. C. Selhuber-Unkel, T. Spratte, C. Vazquez Martel, and B. Weidinger (Heidelberg University) for the fruitful discussions.

Conflict of Interest

The authors declare no conflict of interest.

Data Availability Statement

The data that support the findings of this study are available in the supplementary material of this article.

Keywords

3D laser lithography, alkoxyamines, covalent adaptable networks, dynamic covalent chemistry, nitroxide mediated polymerization (NMP), two photon printing

Received: July 8, 2022
Revised: August 26, 2022
Published online:

[1] M. Medina-Sánchez, V. Magdanz, M. Guix, V. M. Fomin, O. G. Schmidt, *Adv. Funct. Mater.* **2018**, *28*, 1707228.
[2] S. Nocentini, C. Parmeggiani, D. Martella, D. S. Wiersma, *Adv. Optical Mater.* **2018**, *6*, 1800207.
[3] J. Shintake, V. Cacucciolo, D. Floreano, H. Shea, *Adv. Mater.* **2018**, *30*, 1707035.
[4] N. Vanparijs, L. Nuhn, B. G. De Geest, *Chem. Soc. Rev.* **2017**, *46*, 1193.
[5] Y. Chao, Q. Chen, Z. Liu, *Adv. Funct. Mater.* **2020**, *30*, 1902785.
[6] R. D. Field, P. N. Anandakumaran, S. K. Sia, *Appl. Phys. Rev.* **2019**, *6*, 041305.
[7] S. C. Ligon, R. Liska, J. Stampfl, M. Gurr, R. Mülhaupt, *Chem. Rev.* **2017**, *117*, 10212.
[8] S. Maruo, O. Nakamura, S. Kawata, *Opt. Lett.* **1997**, *22*, 132.
[9] C. Barner-Kowollik, M. Bastmeyer, E. Blasco, G. Delaittre, P. Müller, B. Richter, M. Wegener, *Angew. Chem., Int. Ed.* **2017**, *56*, 15828.
[10] M. Carlotti, V. Mattoli, *Small* **2019**, *15*, 1902687.
[11] F. Jin, J. Liu, Y.-Y. Zhao, X.-Z. Dong, M.-L. Zheng, X.-M. Duan, *Nat. Commun.* **2022**, *13*, 1357.
[12] W. Gao, H. Chao, Y.-C. Zheng, W.-C. Zhang, J. Liu, F. Jin, X.-Z. Dong, Y.-H. Liu, S.-J. Li, M.-L. Zheng, *ACS Appl. Mater. Interfaces* **2021**, *13*, 27796.
[13] T.-Y. Huang, M. S. Sakar, A. Mao, A. J. Petruska, F. Qiu, X.-B. Chen, S. Kennedy, D. Mooney, B. J. Nelson, *Adv. Mater.* **2015**, *27*, 6644.
[14] I. C. Yasa, A. F. Tabak, O. Yasa, H. Ceylan, M. Sitti, *Adv. Funct. Mater.* **2019**, *29*, 1808992.
[15] Z. Lao, N. Xia, S. Wang, T. Xu, X. Wu, L.i Zhang, *Micromachines* **2021**, *12*, 465.
[16] J. Knoška, L. Adriano, S. Awel, K. Beyerlein, O. Yefanov, D. Oberthuer, G. E. Peña Murillo, N. Roth, I. Sarrou, P. Villanueva-Perez, M. O. Wiedorn, F. Wilde, S. Bajt, H. N. Chapman, M. Heymann, *Nat. Commun.* **2020**, *11*, 657.
[17] A. Barbot, D. Wales, E. Yeatman, G.-Z. Yang, *Adv. Sci.* **2021**, *8*, 2004643.
[18] a) J. Li, S. Thiele, R. W. Kirk, B. C. Quirk, A. Hoogendoorn, Y. C. Chen, K. Peter, S. J. Nicholls, J. W. Verjans, P. J. Psaltis, C. Bursill, A. M. Herkommer, H. Giessen, R. A. McLaughlin, *Small* **2022**, *18*, 2107032; b) P. Ruchka, S. Hammer, M. Rockenhäuser, R. Albrecht, J. Drozella, S. Thiele, H. Giessen, T. Langen, *Quantum Sci. Technol.* **2022**, *7*, 045011.
[19] A. Kubec, M.-C. Zdora, U. T. Sanli, A. Diaz, J. Vila-Comamala, C. David, *Nat. Commun.* **2022**, *13*, 1305.
[20] C. A. Spiegel, M. Hippler, A. Münchinger, M. Bastmeyer, C. Barner-Kowollik, M. Wegener, E. Blasco, *Adv. Funct. Mater.* **2020**, *30*, 1907615.

[21] X. Kuang, D. J. Roach, J. Wu, C. M. Hamel, Z. Ding, T. Wang, M. L. Dunn, H. J. Qi, *Adv. Funct. Mater.* **2018**, *29*, 1805290.
[22] M. del Pozo, J. A. H. P. Sol, A. P. H. J. Schenning, M. G. Debije, *Adv. Mater.* **2022**, *34*, 2104390.
[23] Y. Dong, S. Wang, Y. Ke, L. Ding, X. Zeng, S. Magdassi, Y. Long, *Adv. Mater. Technol.* **2020**, *5*, 2000034.
[24] M. Champeau, D. A. Heinze, T. N. Viana, E. R. de Souza, A. C. Chinellato, S. Titotto, *Adv. Funct. Mater.* **2020**, *30*, 1910606.
[25] D. Jin, Q. Chen, T.-Y. Huang, J. Huang, L. Zhang, H. Duan, *Mater. Today* **2020**, *32*, 19.
[26] M. Hippler, E. Blasco, J. Qu, M. Tanaka, C. Barner-Kowollik, M. Wegener, M. Bastmeyer, *Nat. Commun.* **2019**, *10*, 232.
[27] J.-Y. Wang, F. Jin, X.-Z. Dong, J. Liu, M.-L. Zheng, *Adv. Mater. Technol.* **2022**, *7*, 2200276.
[28] C. Zheng, F. Jin, Y. Zhao, M. Zheng, J. Liu, X. Dong, Z. Xiong, Y. Xia, X. Duan, *Sens. Actuators, B* **2020**, *304*, 127345.
[29] H. Zeng, P. Wasylczyk, C. Parmeggiani, D. Martella, M. Burresi, D. S. Wiersma, *Adv. Mater.* **2015**, *27*, 3883.
[30] A. Münchinger, V. Hahn, D. Beutel, S. Woska, J. Monti, C. Rockstuhl, E. Blasco, M. Wegener, *Adv. Mater. Technol.* **2022**, *7*, 2100944.
[31] W. Zhang, H. Wang, H. Wang, J. Y. E. Chan, H. Liu, B. Zhang, Y. F. Zhang, K. Agarwal, Y. Yang, A. S. Ranganath, H. Y. Low, Q. Ge, J. K. W. Yang, *Nat. Commun.* **2021**, *12*, 112.
[32] C. A. Spiegel, M. Hackner, V. P. Bothe, J. P. Spatz, E. Blasco, *Adv. Funct. Mater.* **2022**, 2110580.
[33] M. P. Jeske, W. Zhang, M. Anthamatten, *Adv. Mater. Technol.* **2022**, *7*, 2101725.
[34] C. J. Kloxin, C. N. Bowman, *Chem. Soc. Rev.* **2013**, *42*, 7161.
[35] J. M. Winne, L. Leibler, F. E. Du Prez, *Polym. Chem.* **2019**, *10*, 6091.
[36] T. Maeda, H. Otsuka, A. Takahara, *Prog. Polym. Sci.* **2009**, *34*, 581.
[37] B. Zhang, K. Kowsari, A. Serjouei, M. L. Dunn, Q. Ge, *Nat. Commun.* **2018**, *9*, 1831.
[38] A. Durand-Silva, K. P. Cortés-Guzmán, R. M. Johnson, S. D. Perera, S. D. Diwakara, R. A. Smaldone, *ACS Macro Lett.* **2021**, *10*, 486.
[39] Z. Zhang, N. Corrigan, C. Boyer, *Angew. Chem., Int. Ed.* **2022**, *61*, e202114111.
[40] Y. Amamoto, H. Otsuka, A. Takahara, K. Matyjaszewski, *Adv. Mater.* **2012**, *24*, 3975.
[41] Y. Jia, Y. Matt, Q. An, I. Wessely, H. Mutlu, P. Theato, S. Bräse, A. Llevot, M. Tsotsalas, *Polym. Chem.* **2020**, *11*, 2502.
[42] J. J. Cash, T. Kubo, A. P. Bapat, B. S. Sumerlin, *Macromolecules* **2015**, *48*, 2098.
[43] N. Zheng, Y. Xu, Q. Zhao, T. Xie, *Chem. Rev.* **2021**, *121*, 1716.
[44] Q. An, I. D. Wessely, Y. Matt, Z. Hassan, S. Bräse, M. Tsotsalas, *Polym. Chem.* **2019**, *10*, 672.
[45] Z. Ding, L. Yuan, G. Liang, A. Gu, *J. Mater. Chem. A* **2019**, *7*, 9736.
[46] C. J. Hawker, A. W. Bosman, E. Harth, *Chem. Rev.* **2001**, *101*, 3661.
[47] C. J. Hawker, *Acc. Chem. Res.* **1997**, *30*, 373.
[48] K. Jin, L. Li, J. M. Torkelson, *Adv. Mater.* **2016**, *28*, 6746.
[49] G. Audran, P. Brémond, S. R. A. Marque, *Chem. Commun.* **2014**, *50*, 7921.
[50] Y. Jia, G. Delaittre, M. Tsotsalas, *Macro. Mat. and Eng.* **2022**, 202200178.
[51] H. Otsuka, *Polym. J.* **2013**, *45*, 879.
[52] B. Schulte, M. Tsotsalas, M. Becker, A. Studer, L. De Cola, *Angew. Chem., Int. Ed.* **2010**, *49*, 6881.
[53] I. Wessely, V. Mugnaini, A. Bihlmeier, G. Jeschke, S. Bräse, M. Tsotsalas, *RSC Adv.* **2016**, *6*, 55715.
[54] I. D. Wessely, Y. Matt, Q. An, S. Bräse, M. Tsotsalas, *RSC Adv.* **2021**, *11*, 27714.
[55] T. S. Fischer, S. Spann, Q. An, B. Luy, M. Tsotsalas, J. P. Blinco, H. Mutlu, C. Barner-Kowollik, *Chem. Sci.* **2018**, *9*, 4696.
[56] P. Kiefer, V. Hahn, M. Nardi, L. Yang, E. Blasco, C. Barner-Kowollik, M. Wegener, *Adv. Opt. Mater.* **2020**, *8*, 2000895.
[57] H. Yagyu, Y. Hirai, A. Uesugi, Y. Makino, K. Sugano, T. Tsuchiya, O. Tabata, *Polymer* **2012**, *53*, 4834.
[58] K. Hagita, H. Morita, M. Doi, H. Takano, *Macromolecules* **2016**, *49*, 1972.
[59] K. Kremer, G. S. Grest, *J. Chem. Phys.* **1990**, *92*, 5057.
[60] E. Sedghamiz, M. Liu, W. Wenzel, *Nat. Commun.* **2022**, *13*, 2115.
[61] M. Tehrani, A. Sarvestani, *Eur. Polym. J.* **2017**, *87*, 136.
[62] W. C. Oliver, G. M. Pharr, *J. Mater. Res.* **1992**, *7*, 1564.
[63] B. Button, L. H. Cai, C. Ehre, M. Kesimer, D. B. Hill, J. K. Sheehan, R. C. Boucher, M. Rubinstein, *Sci.* **2012**, *337*, 937.
[64] D. Frenkel, B. Smit, M. A. Ratner, *Understanding molecular simulation: from algorithms to applications*, Academic press, San Diego **1996**.
[65] D. C. Prieve, W. B. Russel, *J. Colloid Interf. Sci.* **1988**, *125*, 1.
[66] D. R. H. R. Tretyakov, *J. Chem. Phys.* **2009**, *130*, 234101.
[67] M. Wei, P. Xu, Y. Yuan, X. Tian, J. Sun, J. Lin, *Phys. Chem. Chem. Phys.* **2018**, *20*, 8228.
[68] J. Gao, J. H. Weiner, *J. Chem. Phys.* **1995**, *103*, 1614.